

## Shear activation of mechanophore-crosslinked polymers†

Cassandra M. Kingsbury,<sup>ad</sup> Preston A. May,<sup>bd</sup> Douglas A. Davis,<sup>bd</sup> Scott R. White,<sup>cd</sup> Jeffrey S. Moore<sup>abd</sup>  
and Nancy R. Sottos<sup>\*ad</sup>

Received 19th November 2010, Accepted 24th January 2011

DOI: 10.1039/c0jm04015k

A new strategy is employed to impart productive mechanochemical response to crosslinked polymers. Force-sensitive molecules, termed mechanophores, are successfully incorporated as crosslinkers into poly(methyl methacrylate) through a free radical polymerization initiated with benzoyl peroxide and *N,N*-dimethylaniline. Evidence of a shear activated local chemical reaction (an electrocyclic ring opening) is provided by a color- and fluorescence-generating spiropyran mechanophore. Bulk polymer samples and controls were studied under shear loading. *In situ* full field fluorescence imaging is used to determine the threshold stress and strain required for activation as a function of shear rate and polymer architecture, both of which have a significant effect on mechanochemical activity in the bulk polymer. Increasing the shear rate leads to an increase in activation stress, similar to bulk polymer yielding. Increasing the length of the primary crosslinker with respect to the spiropyran leads to a decrease in activation stress, while the activation strain becomes more shear rate dependent with longer primary crosslinkers. These findings show that the molecular details of the network architecture can be altered to tune the mechanochemical response.

## Introduction

Stimuli responsive materials adapt their properties or alter their form in response to a change in environment. Responses coupled to a wide range of external stimuli such as temperature, UV and visible light, pH, electric potential, magnetic field and biological analytes have been demonstrated in polymers.<sup>1</sup> These responses include changes in optical properties, mechanical properties, chemical composition, shape, volume, surface tension, permeability, adhesive and adsorptive properties, and degradation. Some of the most extensively studied polymers are polymer brushes,<sup>2</sup> hydrogels,<sup>3</sup> and shape memory polymers.<sup>4</sup> Inspired by mechanotransduction in biological systems,<sup>5</sup> an emerging class of stimuli responsive polymers responds chemically to mechanical forces.<sup>6</sup> The default mechanochemical reaction to external stress is unselective homolytic bond scission,<sup>7</sup> which ultimately results in failure of polymeric materials. Mechanochemical degradation of polymer chains has been widely studied,<sup>8–11</sup> but recent investigations have focused on the productive channeling of

mechanical energy to activate chemical pathways that favorably alter or enhance the material properties of the polymer. Successful strategies for the development of mechanosensitive polymers include the aggregation of photoluminescent dyes,<sup>12</sup> *cis-trans* isomerization of azobenzenes,<sup>13</sup> supramolecular re-organization of poly(urethane-diacetylene) chain segments,<sup>14</sup> distortion of polymerized crystalline colloidal arrays,<sup>15</sup> deformation-induced ion-pair dissociation,<sup>16,17</sup> mechanical breakup of cinnamoyl groups,<sup>18</sup> and activation of force-sensitive molecules, *i.e.*, mechanophores, linked into the polymer backbone.<sup>19–25</sup>

Hickenboth *et al.*<sup>19</sup> first demonstrated force-induced ring opening of a poly(ethylene glycol) (PEG)-linked benzocyclobutene mechanophore in solution, revealing that force was capable of altering the course of normal thermal reaction pathways. Ong *et al.*<sup>26</sup> analyzed this mechanophore computationally, showing mechanical force could produce products not achievable by other pathways. Force-biased electrocyclic ring opening was also observed by Lenhardt and co-workers<sup>21</sup> during the mechanoactivation of *cis-* and *trans gem*-dichlorocyclopropane-linked polymers. Dicyanocyclo-butane mechanophores linked in poly(methyl acrylate) (PMA) have also been shown to form cyanoacrylate groups under the action of mechanical force.<sup>22</sup>

Potisek *et al.*<sup>20</sup> investigated mechanical activation of spiropyran-linked PMA in solution. This mechanophore reversibly transformed from a closed, colorless spiropyran (SP) form to a highly colored and fluorescent merocyanine (MC) structure by rupture of the spiro carbon–oxygen (C–O) bond. Davis *et al.*<sup>23</sup> showed selective activation of the SP mechanophore linked in linear PMA, as well as in crosslinked poly(methyl methacrylate)

<sup>a</sup>Department of Materials Science and Engineering, University of Illinois at Urbana-Champaign, 1304 W. Green Street, Urbana, IL, 61801, USA

<sup>b</sup>Department of Chemistry, University of Illinois at Urbana-Champaign, 505 S. Mathews Avenue, Urbana, IL, 61801, USA

<sup>c</sup>Department of Aerospace Engineering, University of Illinois at Urbana-Champaign, 104 S. Wright Street, Urbana, IL, 61801, USA

<sup>d</sup>Beckman Institute for Advanced Science and Technology, University of Illinois at Urbana-Champaign, 405 N. Mathews Avenue, Urbana, IL, 61801, USA. E-mail: n-sottos@illinois.edu

† Electronic supplementary information (ESI) available. See DOI: 10.1039/c0jm04015k

(PMMA) polymeric materials. A recent review of stress-responsive materials<sup>27</sup> called for the need for more fundamental and quantitative knowledge of mechanophore activity. In an attempt to quantitatively probe mechanophore responses, SP has been incorporated in polycaprolactone<sup>24</sup> to measure the force-induced by SP opening and closing, and polyurethane<sup>25</sup> to measure the change in the energy landscape of SP under mechanical load.

In the current work, we explored in detail the force-induced behavior of mechanophore-crosslinked PMMA bulk polymers under shear loading to more accurately determine a threshold stress and strain for mechanochemical activation. The mechanophore in this study was the previously synthesized di-acrylate spiropyran.<sup>23</sup> As shown in Fig. 1a and b, three different primary crosslinkers of varying length were investigated with the goal of changing the molecular architecture to enhance load transfer to the mechanophores. New test protocols were developed to elucidate the effect of polymer architecture and strain rate on the threshold values of stress and strain required for activation.

## Experimental procedures

### Materials and synthesis

The material investigated was a crosslinked poly(methyl methacrylate) (PMMA) with a total crosslink density of 1 mol%, which was kept constant for all samples. PMMA samples were crosslinked with both a primary crosslinker (0.982 mol%) and a secondary crosslinker of spiropyran (**1**) (0.018 mol%). Mechanophore content was chosen based on a previous study of

this polymer system.<sup>23</sup> The primary crosslinker was either ethylene glycol dimethacrylate (EGDMA) (**3**), poly(ethylene glycol) dimethacrylate with a molecular weight of 550 Da and a polydispersity index (PDI) of 1.02 (PEG550) (**4**) or poly(ethylene glycol) dimethacrylate with a molecular weight of 750 Da and a PDI of 1.04 (PEG750) (**5**). The approximate fully extended lengths and chemical structures of each primary crosslinker along with the closed and open form of the spiropyran mechanophore are given in Fig. 1.

Active polymers (shown in Fig. 1a and b) consisted of difunctional spiropyran (**1**) as the mechanophore and EGDMA (**3**), PEG550 (**4**) or PEG750 (**5**) as the primary crosslinker. Here, polymer was linked to the 5' and 8 attachment points of spiropyran as shown in Fig. 1a, allowing force transfer across the C–O spiro-bond. Monofunctional control polymers (shown in Fig. 1c) were synthesized with monofunctional spiropyran (**6**) and a primary crosslinker of EGDMA (**3**), PEG550 (**4**) or PEG750 (**5**). In this case, polymer was only linked to one attachment point on the spiropyran, precluding force transfer across the molecule. Monofunctional control spiropyran was still reactive to heat and light stimuli, but not mechanical force.<sup>20,23</sup>

Synthesis of the crosslinked PMMA was performed *via* a free radical polymerization using benzoyl peroxide (BPO) as the radical source and *N,N*-dimethylaniline (DMA) as the activator.<sup>23</sup> Unless otherwise stated, all starting materials and reagents were obtained from commercial suppliers and used without further purification. BPO was re-precipitated from acetone using water and partially dried under vacuum. DMA was distilled under reduced pressure from zinc metal. Methyl methacrylate monomer was filtered through a plug of basic

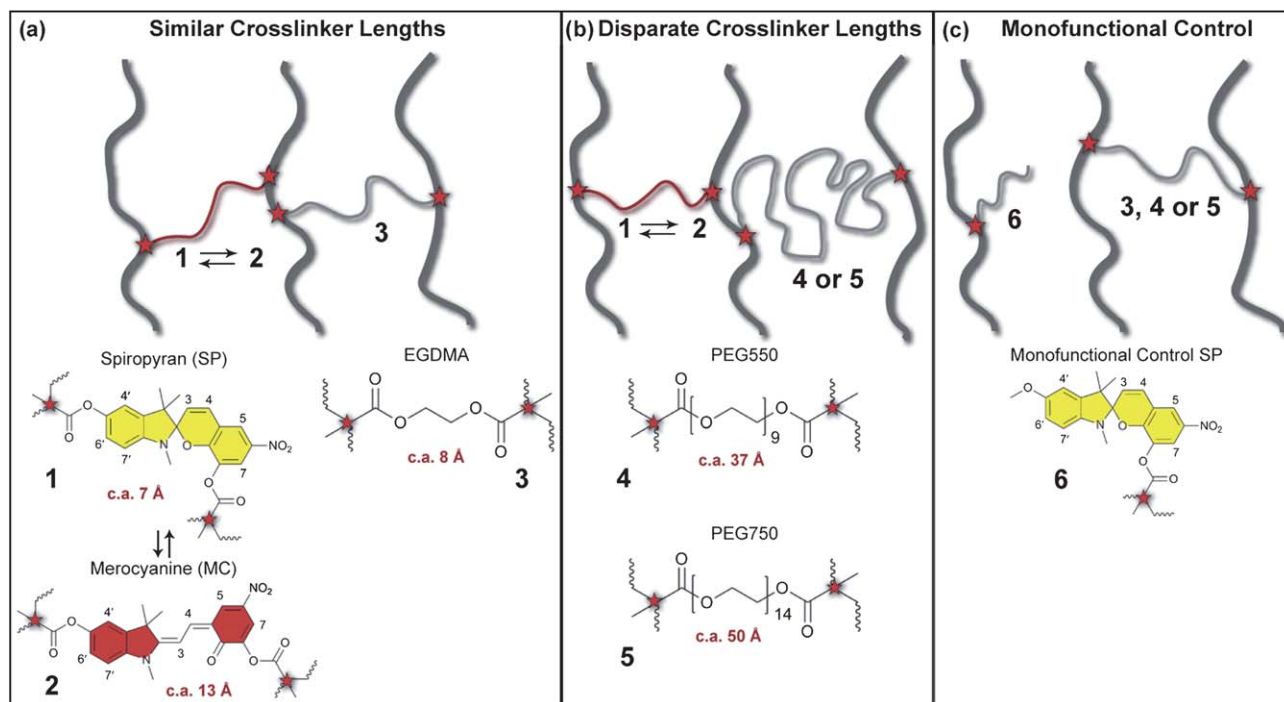


**Fig. 1** PMMA network and crosslinker structures. (a) Schematic of crosslinked PMMA with primary crosslinkers approximately the same length as SP. (b) Schematic of crosslinked PMMA with primary crosslinkers longer than SP. (c) Structure of monofunctional control sample showing SP linked on one side only. Lengths listed are distances between crosslink points (marked by ★) and are coarse estimates from fully extended chains after an energy minimization using Chem 3D.

alumina just before use to remove the inhibitor. Polypropylene syringes (1 mL) with a molded gauge section were used as molds for the polymer.

For mechanically active samples, BPO (15 mg, 0.0619 mmol, 0.00662 equiv.), difunctional spiropyran (**1**) (0.83 mg, 0.00169 mmol, 0.00018 equiv.) and methyl methacrylate (MMA) (1 mL, 9.39 mmol, 1 equiv.) were combined in an Eppendorf tube, flushed with argon for 15 seconds, sealed and mixed. Either EGDMA (**3**) (17.4  $\mu\text{L}$ , 0.0922 mmol, 0.00982 equiv.), PEG550 (**4**) (46.2  $\mu\text{L}$ , 0.0922 mmol, 0.00982 equiv.) or PEG750 (**5**) (62.3  $\mu\text{L}$ , 0.0922 mmol, 0.00982 equiv.) was then added. Once the components were fully dissolved, DMA (6  $\mu\text{L}$ , 0.0473 mmol, 0.00506 equiv.) was added and the Eppendorf tube was again flushed with argon, sealed and mixed. The reaction mixture was allowed to pre-polymerize for 20 minutes to increase viscosity and then injected into the pre-shaped syringe molds while flushing with argon to remove oxygen from the mold and ensure consistent polymerization. After injection, the upper atmosphere of the mold was filled with a blanket of argon. The syringe was then capped with a septum, and the entire mold up to the septum was submerged in a graduated cylinder filled with 25 °C water to mitigate the exotherm of the polymerization. After polymerizing for at least 16 hours, the samples were removed from the syringe molds by cutting and peeling the molds away. Samples were then exposed to intense white light for at least 24 hours to ensure the spiropyran was in the closed form when shear testing began.

Monofunctional control samples were prepared in the same manner except 0.01 molar equivalents of EGDMA (**3**), PEG550 (**4**) or PEG750 (**5**) were used to achieve a crosslink density of 1 mol%. Monofunctional spiropyran (**6**) was added in the same molar ratio as the mechanically active samples (0.00018 equiv.) and was dissolved in 100  $\mu\text{L}$  of dichloromethane before injection into the reaction mixture to enhance solubility. Furthermore, plain control samples were prepared with 0.01 molar equivalents of EGDMA (**3**), PEG550 (**4**) or PEG750 (**5**) and no spiropyran.

### Shear testing and data analysis

Shear testing was performed with a TA Instrument's AR-G2 rheometer. Custom torsion grips were designed and fabricated to hold a cylindrical torsion sample as shown in Fig. 2a. The torsion

sample had a gauge section 2 mm in diameter and 10 mm long, while the grip section of the sample was 4 mm in diameter. Torsion tests were conducted at constant shear rates of 0.001, 0.01, and 0.1  $\text{rad s}^{-1}$ , at room temperature. For all tests, the sample was held in  $2 \text{ N} \pm 0.5 \text{ N}$  tension while rotating at a constant shear rate until failure.

Torsion testing of the lightly crosslinked PMMA produced large deformations that required the use of nonlinear analysis to accurately calculate shear stress and shear strain. We adopted a modification of Nadai's well known solution<sup>28</sup> that incorporated axial strain. The modified shear stress,  $\tau$ , as derived by Wu *et al.*<sup>29</sup> is,

$$\tau = \frac{1}{2\pi r^3} \left( 3M + \theta \frac{dM}{d\theta} \right) \left( \frac{1}{1 - \frac{1}{2} \left( 3A(\theta) + \theta \frac{dA(\theta)}{d\theta} \right)} \right) \quad (1)$$

where  $r$  is the sample radius,  $M$  is the applied torque,  $A$  is the axial strain as a function of rotation, and  $\theta$  is the angle of rotation of the specimen. The corresponding shear strain,  $\gamma$ , is,

$$\gamma = r \left( 1 - \frac{1}{2} A(\theta) \right) \theta. \quad (2)$$

Raw torque and rotation data were collected from the experiment. For this analysis, the change in torque with the change in rotation ( $dM/d\theta$ ) in eqn (1) was calculated as the tangent slope of the torque–rotation curve, and the axial strain was monitored by the distance between the rheometer grips. Shear stress and shear strain were calculated using this raw data and eqn (1) and (2), respectively.

### Full field fluorescence imaging

Excitation and emission spectra of both PMMA–EGDMA and PMMA–PEG were obtained using a Photon Technology International QM-1 fluorimeter. For both polymer types, the excitation peak is centered at approximately 540 nm and the emission peak is centered at approximately 610 nm. Knowing the excitation and emission wavelengths, full field fluorescence (FFF) imaging was accomplished *in situ* during torsion testing. A schematic diagram of the FFF setup is shown in Fig. 2b. The

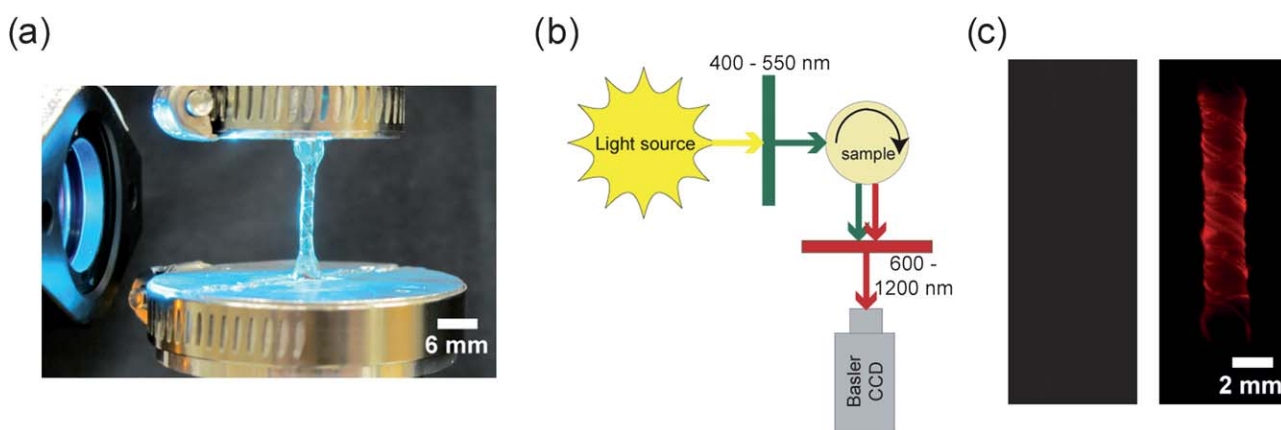


**Fig. 2** Full field fluorescence imaging technique. (a) Torsion sample in rheometer illuminated with 400–550 nm light, (b) top view of FFF schematic, and (c) typical FFF images before (left) and after (right) testing.

sample was illuminated with a white pipe light that was filtered to allow only 400–550 nm light to pass (Fig. 2a). A Basler CCD camera was positioned at 90° to the illumination source and a filter was used to collect only 600–1200 nm reflected light. Representative images obtained by FFF before and after testing are shown in Fig. 2c. Polymer samples were fully bleached before testing and initial FFF images appeared black. As the SP opened to the MC form and subsequently fluoresced, the polymer gauge section became a vibrant red color in the FFF setup. FFF images were acquired simultaneously with torque–rotation data.

### Confocal imaging

Samples were imaged postmortem using a Leica DMIRE2 laser scanning confocal fluorescence microscope. After testing, samples were sectioned in the activated gauge section using a Buehler Isomet 1000 precision saw to create small cylinders with parallel faces. Planar images of the cylinder cross-section were obtained at a depth of 500  $\mu\text{m}$  below the cut surface to remove any fluorescence due to cutting. Specimens were simultaneously illuminated with wavelengths of 488 nm, 514 nm and 543 nm and fluorescence emission wavelengths of 590–640 nm were collected. Cross-sectional fluorescent images were analyzed using an image analysis program (ImageJ 1.42q). Sixteen line scans were taken from the center of the sample outward radially at angles between 0° and 360°. Line scans were averaged to obtain cross-sectional intensity profiles.

## Results and discussion

### Stress–strain response

Constant shear rate tests in the rheometer produced a brilliant purple color in the gauge section of active samples, indicating activation of the SP mechanophore. To ensure that the conversion of SP to MC during torsion was due to mechanical force, control samples were tested under the same conditions. In great contrast to the active samples, both the monofunctional (6) and spiropyran-free PMMA control samples exhibited no color change in the gauge section of the sample. Fig. 3 shows representative optical images of active, monofunctional control and spiropyran-free control samples before and after testing at each shear rate for PMMA–EGDMA. Although not shown, specimens with a primary crosslinker of PEG550 or PEG750 produced similar results.

Each polymer type was tested using a dynamic temperature ramp in the rheometer to find the room temperature shear storage modulus ( $G'$ ) and the glass transition temperature ( $T_g$ ).  $G'$  was calculated as the average of the shear storage modulus between 25 °C and 30 °C.  $T_g$  was determined based on the temperature for which  $\tan \delta (G'/G'')$  reached a maximum. Table 1 summarizes the data for PMMA crosslinked with each primary crosslinker containing active (1), monofunctional control (6) and no SP. Increasing the length of the primary crosslinker from EGDMA (3) to PEG550 (4) to PEG750 (5) led to a reduction in both  $G'$  and  $T_g$ . This reduction in  $G'$  and  $T_g$  was anticipated since

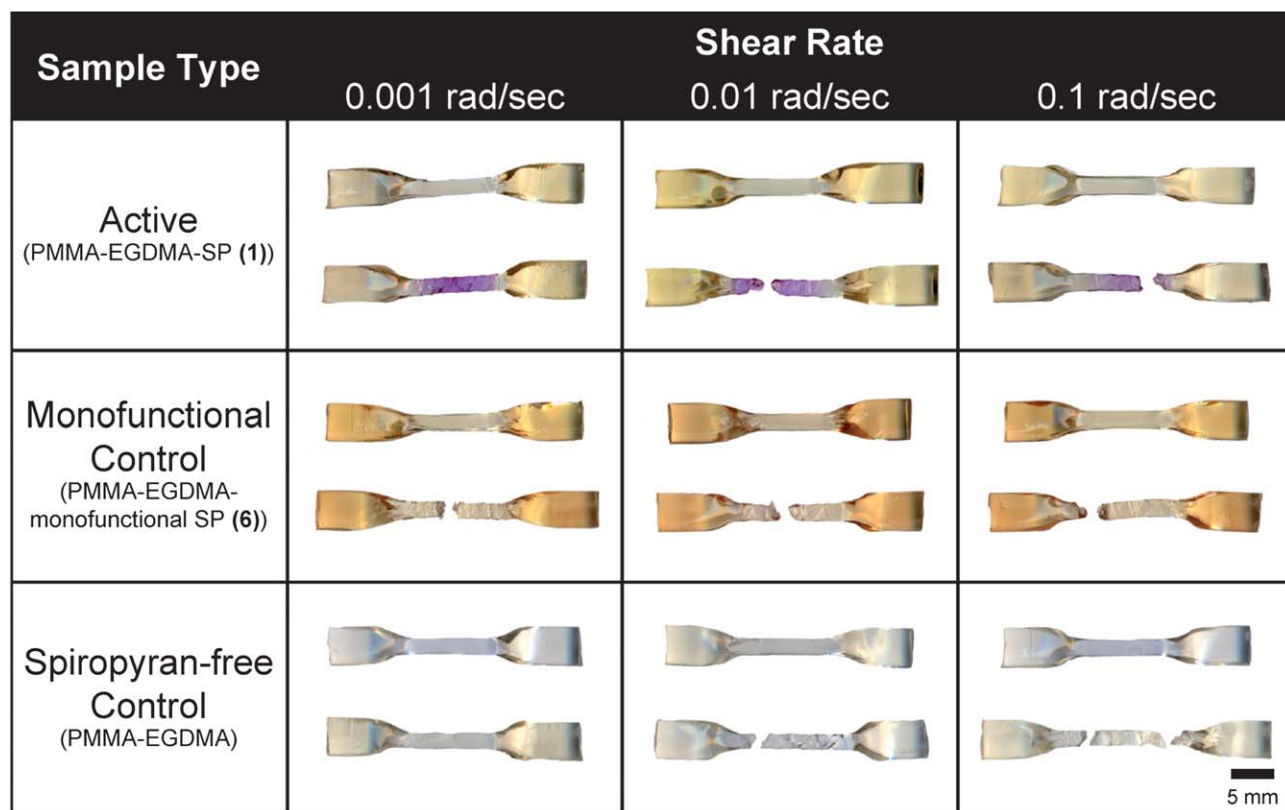


**Fig. 3** Optical images of PMMA–EGDMA samples before (top) and after (bottom) torsional testing. Active samples display intense color change in the gauge section for all shear rates tested, while both control samples do not.

**Table 1** Shear storage modulus and glass transition temperature for various polymer architectures containing either active (1), monofunctional control (6) or no spirocyan

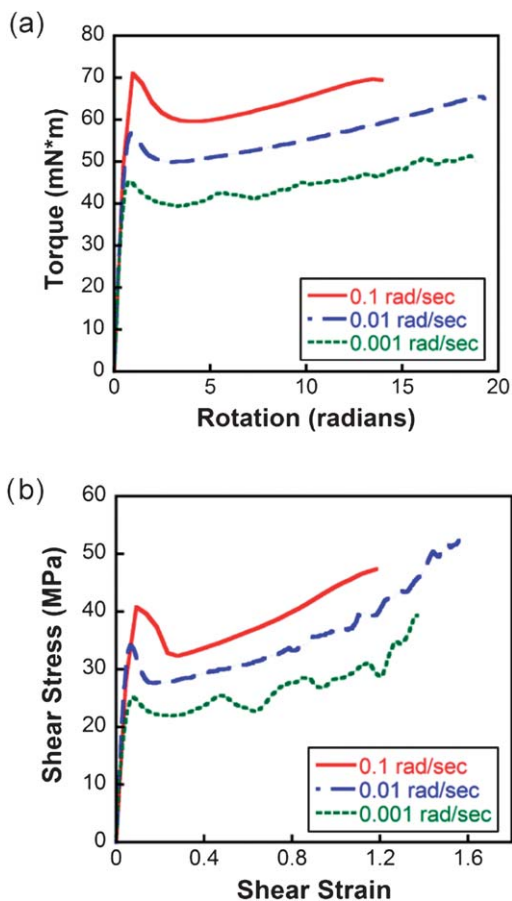
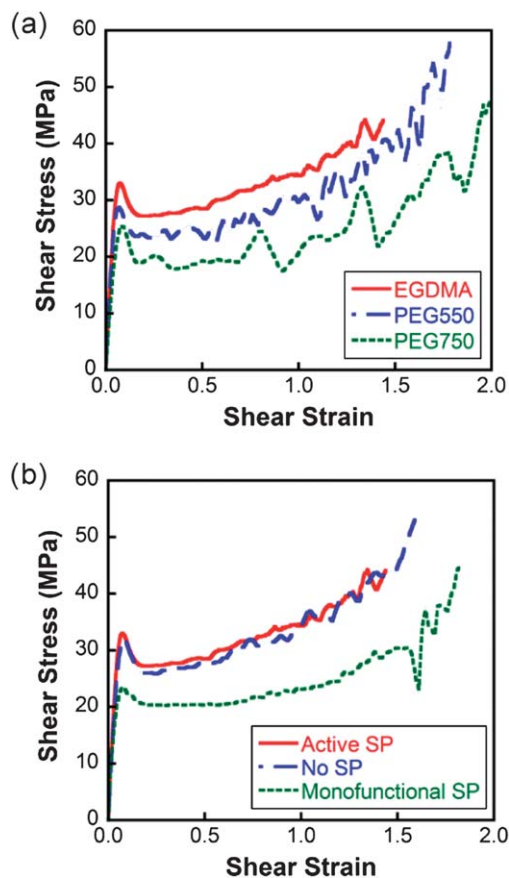
	PMMA-EGDMA			PMMA-PEG550			PMMA-PEG750		
	Active SP	Monofunctional SP	No SP	Active SP	Monofunctional SP	No SP	Active SP	Monofunctional SP	No SP
$G'/\text{GPa}$	1.5	1.7	1.4	1.4	1.0	1.4	1.1	0.8	1.3
$T_g/^\circ\text{C}$	127	92	128	121	91	128	119	82	121

the average molar mass between crosslink points increased.<sup>30,31</sup> Adding active spirocyan (1) had almost no effect on  $G'$  and  $T_g$ , while incorporating monofunctional spirocyan (6) lowered  $T_g$  for all polymer types.

Representative torque-rotation data at three different shear rates are shown in Fig. 4a for active PMMA-EGDMA. The corresponding shear stress-shear strain curves (calculated using eqn (1) and (2)) are shown in Fig. 4b. Similar shear rate trends were also observed for PMMA-PEG550 and PMMA-PEG750. As expected,<sup>32</sup> the shear yield stress, defined as the first local maximum in the shear stress-shear strain curve, increased with increasing shear rate.

Changes in polymer architecture due to the use of different primary and secondary crosslinkers also had a significant effect

on the mechanical behavior of crosslinked PMMA specimens. Fig. 5a summarizes the effect of primary crosslinker length on the mechanical behavior of crosslinked PMMA with active SP (1) at a single shear rate ( $0.01 \text{ rad s}^{-1}$ ). Increasing the length of the primary crosslinker from EGDMA (3) to PEG550 (4) to PEG750 (5) led to a repeatable reduction in shear yield stress. Comparable trends were observed at shear rates of  $0.1 \text{ rad s}^{-1}$  and  $0.001 \text{ rad s}^{-1}$ . The shear stress-shear strain responses of PMMA-EGDMA with active (1), monofunctional control (6) and no SP are compared in Fig. 5b. Incorporation of active SP (1) had little effect on the yield stress, while use of the monofunctional SP (6) led to a significant decrease in yield stress. Similar trends were also recorded for PMMA-PEG550 and PMMA-PEG750 containing the two types of SP. As summarized in Table 1, PMMA

**Fig. 4** Effect of shear rate on mechanical behavior of PMMA-EGDMA. (a) Torque-rotation data as collected during a torsion test. (b) Shear stress-shear strain calculated from the torque-rotation data using eqn (1) and (2).**Fig. 5** Effect of polymer architecture on mechanical behavior. (a) Shear stress-shear strain data at  $0.01 \text{ rad s}^{-1}$  for increasing crosslinker lengths. (b) Shear stress-shear strain data for active PMMA-EGDMA and controls.

specimens synthesized with PEG550, PEG750 and monofunctional SP also had a reduced  $T_g$ . The observed decrease in yield stress for these polymers is consistent with previous studies of polymer yielding at elevated temperatures<sup>33</sup> or as  $T_g - T$  is decreased.<sup>34</sup>

### Activation analysis

Threshold values of the stress and strain required for the onset of mechanochemical activation were obtained through analysis of the FFF images corresponding to discrete points along the stress–strain curves. For each image, intensity was averaged over the field of view and plotted as a function of strain as shown in Fig. 6a. The average intensity was then normalized and fit to a cumulative Weibull curve as shown in Fig. 6b and as described in the ESI†. We defined activation as the point when statistically 1% of the SP was open, or when the normalization factor ( $\bar{I}$ ) equals 0.01. Activation stress and activation strain were determined for each polymer and each shear rate at this activation point.

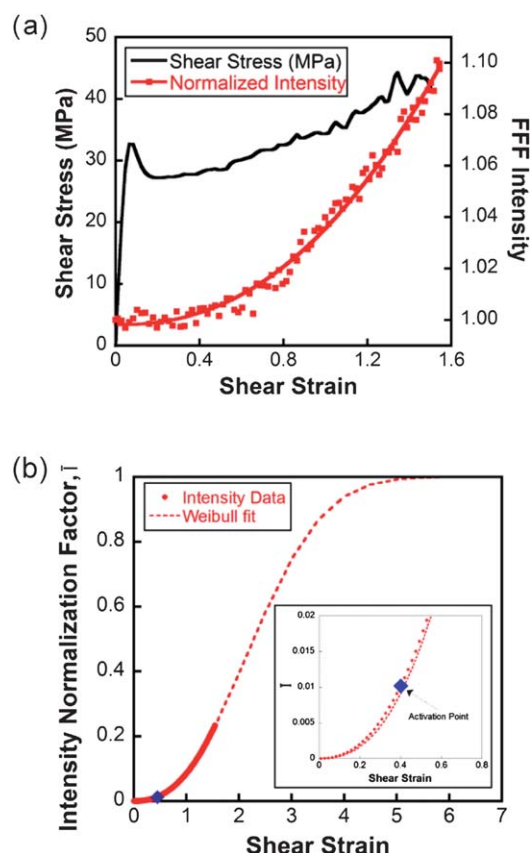


**Fig. 6** Analysis of FFF intensity and application of a cumulative Weibull distribution function. (a) Shear stress–shear strain data correlated with the normalized intensity of FFF images showing an increase in intensity with shear strain for an active sample of PMMA–EGDMA tested at  $0.01 \text{ rad s}^{-1}$ . (b) From the same sample, normalization intensity,  $\bar{I}(\gamma)$  as a function of shear strain fit to a cumulative Weibull distribution function. Inset is an enlarged view of the initial portion of the curve, showing the location of the defined activation point.

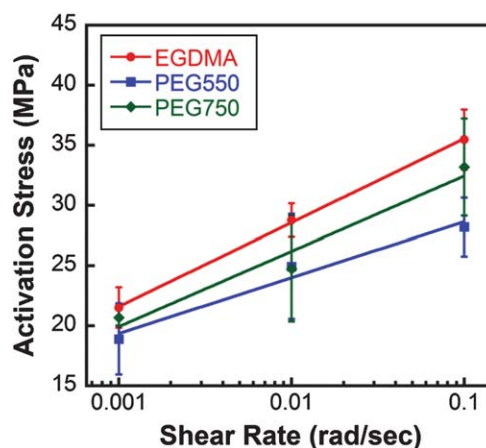


**Fig. 7** Activation stress for each polymer type as a function of shear rate. Error bars reflect one standard deviation of the data.

**Table 2** Activation strain for each polymer type and shear rate. Error is calculated as one standard deviation from the average

Shear rate	PMMA–EGDMA	PMMA–PEG550	PMMA–PEG750
$0.001 \text{ rad s}^{-1}$	$45 \pm 10\%$	$46 \pm 5\%$	$45 \pm 3\%$
$0.01 \text{ rad s}^{-1}$	$46 \pm 6\%$	$45 \pm 11\%$	$67 \pm 7\%$
$0.1 \text{ rad s}^{-1}$	$48 \pm 11\%$	$57 \pm 15\%$	$77 \pm 9\%$

The threshold shear stress for activation is shown in Fig. 7 as a function of shear rate. Activation stress occurred post yield for all active polymers tested, indicating plastic flow was necessary for activation of spiropyran bulk polymers. The need for large deformation is interesting and suggests the significance of molecular motion for activation. Activation stress also increased with increasing shear rate, which mirrored the effect of shear rate on yield stress (Fig. 4b). Polymers with longer primary crosslinkers compared to spiropyran (PMMA–PEG550 and PMMA–PEG750) had a lower activation stress, suggesting enhanced load transfer to the spiropyran mechanophore. However, increasing the crosslinker length from PEG550 to PEG750 resulted in no further reduction in activation stress. Activation strain values and standard deviations for each shear rate and each polymer type are summarized in Table 2. For PMMA–EGDMA and PMMA–PEG550, activation strain was nearly constant across all shear rates. However, PMMA–PEG750 showed some shear rate dependence of activation strain with statistical significance.

### Confocal imaging

Postmortem sectioned samples were imaged to examine the spatial distribution of mechanically activated spiropyran. Confocal images and corresponding intensity profiles of representative samples of PMMA–EGDMA are shown in Fig. 8. The cross-sectional image of an active sample of PMMA–EGDMA (Fig. 8a) reveals a radial gradient in the fluorescence intensity. The fluorescence indicates that activation is spatially non-uniform and largest near the surface. In contrast, the cross-sectional image of the PMMA–EGDMA monofunctional

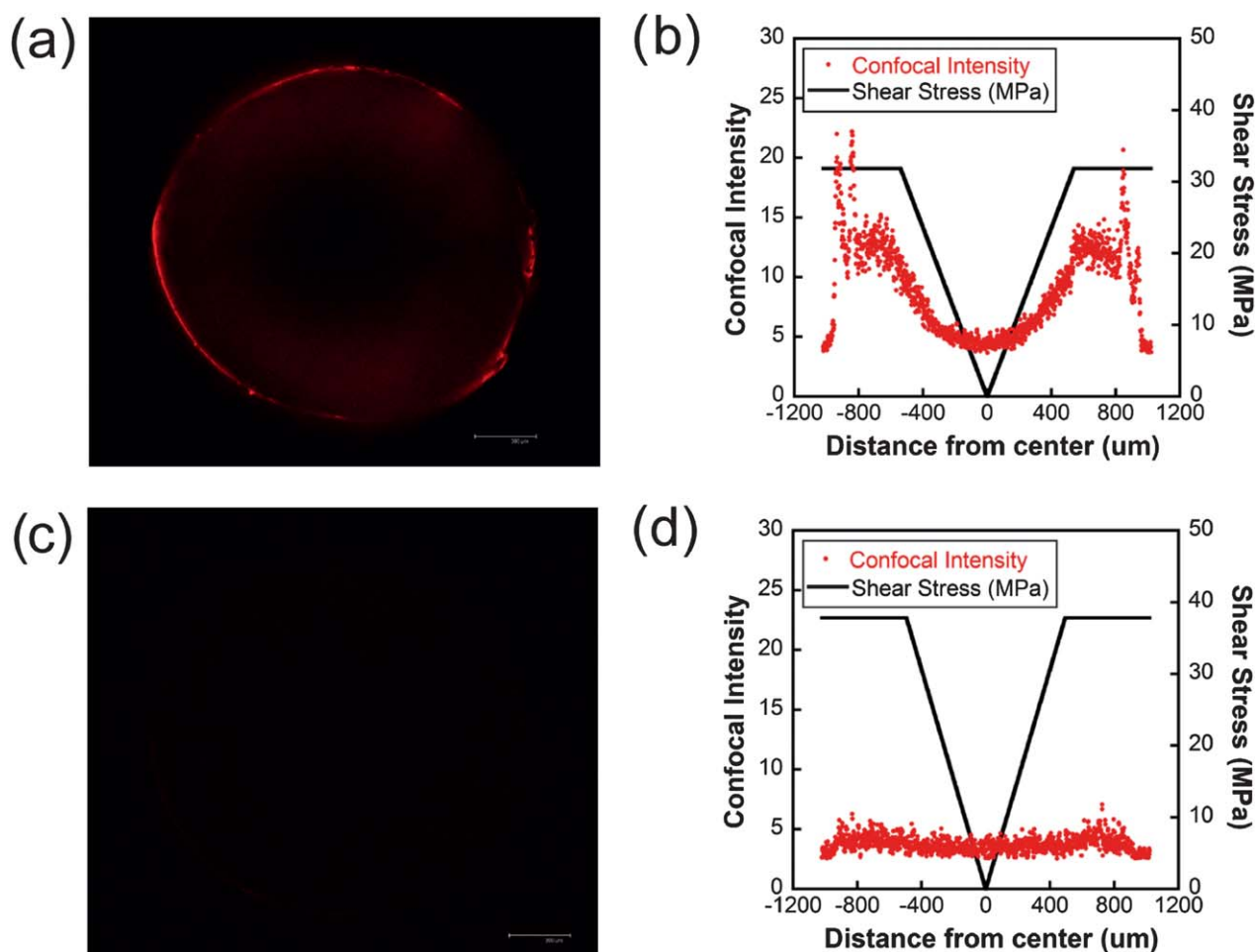


**Fig. 8** Correlation of the cross-sectional confocal fluorescence intensity with the location of the elastic–plastic interface. (a) Cross-sectional confocal fluorescent image of active PMMA–EGDMA (scale bar is 300  $\mu\text{m}$ ). (b) Cross-sectional shear stress profile and intensity map for sample in (a). (c) Cross-sectional confocal fluorescent image of monofunctional control PMMA–EGDMA (scale bar is 300  $\mu\text{m}$ ). (d) Cross-sectional shear stress profile and intensity map for sample in (c).

control sample (Fig. 8c) shows virtually no fluorescence and no preferential gradient of fluorescence intensity across the section.

The distribution of fluorescence intensity across the cross-section is plotted with the corresponding distribution of shear stress in Fig. 8b and d. In the linear-elastic region before yield, shear stress varies linearly with radial position according to:

$$\tau = \frac{2Tx}{\pi r^3} \quad (3)$$

where  $T$  is the torque during testing,  $x$  is the radial distance from the center of the specimen, and  $r$  is the radius of the specimen. Assuming an elastic, perfectly plastic response, the stress remains constant after reaching the yield point as an elastic–plastic interface develops and propagates towards the center of the sample. For each sample, the elastic–plastic interface can be located as the intersection of the shear yield stress and the shear stress variation according to eqn (3).<sup>35</sup> For the active sample (Fig. 8b) a plateau of intensity corresponds to the location of the elastic–plastic interface, while there is no correlation of intensity to the shear stress profile for the case of the monofunctional control sample (Fig. 8d). The correlation of confocal images with

shear stress profiles indicates that large scale mechanochemical activation in these crosslinked polymers is associated with plastic flow.

## Conclusions

The mechanophore-crosslinked PMMA was successfully molded into cylindrical samples with a thin gauge section for torsion testing. Shear loading of active specimens resulted in a brilliant purple color change in the gauge section. *In situ* images were collected throughout testing using a full field fluorescence method. Analysis of the full field fluorescence images enabled measurement of the threshold stress and strain values required for mechanochemical activation as a function of shear rate and different polymer architectures.

Activation of all polymer architectures, at all shear rates, occurred after yield of the bulk polymer. Activation stress increased with increasing shear rate and we infer that the activation stress can be tailored by changing the yield stress of the bulk polymer. The activation strain was nearly constant for PMMA–EGDMA and PMMA–PEG550, but increased slightly

with increasing shear rate for PMMA-PEG750. Control specimens synthesized with monofunctional SP or no SP confirmed that the conversion of SP to MC was caused by mechanical force and not another factor such as heat or UV light.

Confocal imaging revealed strong correlation of cross-sectional fluorescence intensity and location of the elastic-plastic interface. These results lend further evidence that activation of spiropropan occurs by mechanical transduction after yielding and upon large scale plastic flow.

## Acknowledgements

Funding for this research was provided by ARO MURI grant number W911NF-07-1-0409. Confocal imaging was carried out at the Beckman Institute for Advanced Science and Technology at the University of Illinois with the help of the Imaging Technology Group. The authors gratefully acknowledge the University of Illinois' Aerospace Engineering machine shop for providing custom molds and custom torsion grips as well as Dorothy Loudermilk for graphic design.

## References

- 1 M. A. C. Stuart, W. T. S. Huck, J. Genzer, M. Müller, C. Ober, M. Stamm, G. B. Sukhorukov, I. Szleifer, V. V. Tsukruk, M. Urban, F. Winnik, S. Zauscher, I. Luzinov and S. Minko, *Nat. Mater.*, 2010, **9**, 101–113.
- 2 S. Minko, *J. Macromol. Sci., Polym. Rev.*, 2006, **46**, 397–420.
- 3 S. H. Gehrke, *Adv. Polym. Sci.*, 1993, **110**, 81–144.
- 4 M. Behl and A. Lendlein, *Mater. Today*, 2007, **4**, 20–28.
- 5 A. S. French, *Annu. Rev. Physiol.*, 1992, **54**, 135–152.
- 6 M. M. Caruso, D. A. Davis, Q. Shen, S. A. Odom, N. R. Sottos, S. R. White and J. S. Moore, *Chem. Rev.*, 2009, **109**, 5755–5798.
- 7 M. K. Beyer and H. Clausen-Schaumann, *Chem. Rev.*, 2005, **105**, 2921–2948.
- 8 W. Kauzmann and H. Eyring, *J. Am. Chem. Soc.*, 1940, **62**, 3113–3125.
- 9 A. Casale and R. S. Porter, *Polymer Stress Reactions*, Academic Press, New York, 1978, vol. I and II.
- 10 R. S. Porter and A. Casale, *Polym. Eng. Sci.*, 1985, **25**, 129–156.
- 11 H. H. Kausch and C. J. G. Plummer, *Polymer*, 1994, **35**, 3848–3857.
- 12 C. Löwe and C. Weder, *Adv. Mater.*, 2002, **14**, 1625–1629.
- 13 S. Kim and D. H. Reneker, *Polym. Bull.*, 1993, **31**, 367–374.
- 14 R. A. Nallicheri and M. F. Rubner, *Macromolecules*, 1991, **24**, 517–525.
- 15 S. H. Foulger, P. Jiang, A. Lattam, D. W. Smith, Jr and J. Ballato, *Langmuir*, 2001, **17**, 6023–6026.
- 16 O. Azzaroni, B. Trappman, P. van Rijn, F. Zhou, B. Kong and W. T. S. Huck, *Angew. Chem., Int. Ed.*, 2006, **45**, 7440–7443.
- 17 J. E. Comrie and W. T. S. Huck, *Macromol. Rapid Commun.*, 2008, **29**, 539–546.
- 18 S. Cho, J. Kim and C. Chung, *Sens. Actuators, B*, 2008, **134**, 822–825.
- 19 C. R. Hickenboth, J. S. Moore, S. R. White, N. R. Sottos, J. Baudry and S. R. Wilson, *Nature*, 2007, **446**, 423–427.
- 20 S. L. Potisek, D. A. Davis, N. R. Sottos, S. R. White and J. S. Moore, *J. Am. Chem. Soc.*, 2007, **129**, 13808–13809.
- 21 J. M. Lenhardt, A. L. Black and S. L. Craig, *J. Am. Chem. Soc.*, 2009, **131**, 10818–10819.
- 22 M. J. Kryger, M. T. Ong, S. A. Odom, N. R. Sottos, S. R. White, T. J. Martinez and J. S. Moore, *J. Am. Chem. Soc.*, 2010, **132**, 4558–4559.
- 23 D. A. Davis, A. Hamilton, J. Yang, L. D. Cremar, D. Van Gough, S. L. Potisek, M. T. Ong, P. V. Braun, T. J. Martinez, S. R. White, J. S. Moore and N. R. Sottos, *Nature*, 2009, **459**, 68–72.
- 24 G. O'Bryan, B. M. Wong and J. R. McElhanon, *ACS Appl. Mater. Interfaces*, 2010, **2**, 1594–1600.
- 25 C. K. Lee, D. A. Davis, S. R. White, J. S. Moore, N. R. Sottos and P. V. Braun, *J. Am. Chem. Soc.*, 2010, **132**, 16107–16111.
- 26 M. T. Ong, J. Leiding, H. Tao, A. M. Virshup and T. J. Martinez, *J. Am. Chem. Soc.*, 2009, **131**, 6377–6379.
- 27 A. L. Black, J. M. Lenhardt and S. L. Craig, *J. Mater. Chem.*, 2011, **21**, 1655–1663.
- 28 A. Nadai, *Theory of Flow and Fracture of Solids*, McGraw-Hill, New York, 3rd edn, 1950.
- 29 H. C. Wu, Z. Xu and P. T. Wang, *J. Test. Eval.*, 1992, **20**, 396–402.
- 30 P. J. Flory, *Principles of Polymer Chemistry*, Cornell University Press, New York, 1953, ch. 11.
- 31 J. P. Bell, *J. Appl. Polym. Sci.*, 1970, **14**, 1901.
- 32 H. Eyring, *J. Chem. Phys.*, 1936, **4**, 283.
- 33 E. M. Arruda, M. C. Boyce and R. Jayachandran, *Mech. Mater.*, 1995, **19**, 193–212.
- 34 W. D. Cook, A. E. Mayr and G. H. Edward, *Polymer*, 1983, **24**, 292–296.
- 35 D. W. A. Rees, *J. Mech. Eng. Sci.*, 2009, **223**, 557–571.